Chinese Chemical Letters 34 (2023) 108604

Contents lists available at ScienceDirect

Chinese Chemical Letters

journal homepage: www.elsevier.com/locate/cclet

Theoretical study on the application of the largest aluminum-pyrazole ring in electrochemical nitrogen reduction reaction

Zirui Wang[a,b,d,1], Sihao Shen[a,c,1], Yupeng Han[a,c], Weihui Fang[a,c,d,*], Qiaohong Li[a,c,d,*], Jian Zhang[a,c,d]

[a] State Key Laboratory of Structural Chemistry, Fujian Institute of Research on the Structure of Matter, Chinese Academy of Sciences, Fuzhou 350002, China
[b] School of Physical Science and Technology, ShanghaiTech University, Shanghai 201210, China
[c] Chinese Academy of Sciences, University of Chinese Academy of Sciences, Beijing 100049, China
[d] Fujian College, University of Chinese Academy of Sciences, Fuzhou 350002, China

ARTICLE INFO

Article history:
Received 17 March 2023
Revised 22 May 2023
Accepted 24 May 2023
Available online 25 May 2023

Keywords:
Nitrogen reduction reaction
Hydrogen evolution reaction
Electrocatalysts
Density functional theory
Aluminum-pyrazole ring
Metal catalyst

ABSTRACT

Electrochemical nitrogen reduction reaction (NRR) is a mild and sustainable method for ammonia synthesis. Therefore, developing high activity, selectivity, and economic efficiency catalysts with considering the synergistic effects between catalysts and carriers to design novel structural models is very important. Considering the non-noble metal NRR catalyst, Mo_3, we tried to find a suitable carrier which is stable and economical. Herein, we used the largest atomically precise aluminum-pyrazole ring (AlOC-69) to date (diameter up to 2.3 nm). The larger ring cavities and the presence of abundant hydroxy groups make AlOC-69 an ideal molecular carrier model and provide a basis for studying its structure-activity relationship. The formation energy (−0.76 eV) and stable Mo-O bonds indicate that Mo_3 can be stabilized on the $Al_{10}O_{10}$ surface. Additionally, N_2 has fully activated due to the strong interaction between the p-orbital of N and the d-orbital of Mo. The low limiting potential (−0.28 V) emerges that $Mo_3@Al_{10}O_{10}$ has ideal catalytic activity and selectivity. This research provides a promising catalyst model and an understanding of its catalytic process at the atomic level, providing a new approach for the co-design of catalyst and carrier in NRR.

Ammonia (NH_3) is an important industrial chemical used extensively in agricultural fuels, medicines, and fertilizers [1–3]. However, the traditional Haber-Basch process for ammonia synthesis has problems such as high energy consumption and serious pollution [4–6]. The electrochemical synthesis of ammonia has the characteristics of mild conditions, simple and safe process, high activity, and nitrogen reduction reaction (NRR: $N_2 + 6H^+ + 6e^- \rightarrow 2NH_3$) can be carried out at ambient temperature and pressure [7–9]. Therefore, how to design and synthesize an efficient catalyst to reduce the activation energy of electrochemical NRR and inhibit the formation of hydrogen evolution reaction (HER: $2H^+ + 2e^- \rightarrow H_2$) has become an important research focus[8]. Existing electro-catalytic ammonia synthesis catalysts include metal catalysts [7,8,10–18], non-metallic catalysts (such as boron-doped graphene, nitrogen-doped porous carbon, and single-boron) [19–21], polymers (such as polyaniline) [22], and composite catalysts (such as $C_{18}@Fe_3P$) [23], *etc*. Among them, metal catalysts can be divided into noble metal catalysts (such as Ru, Au, Pt, and their alloys) [8,10–12], and non-noble metal catalysts (such as Ni, Mo, and Fe) [7,13–16,24–27]. The high cost and rarity of traditional noble metallic catalysts limit their large application. Consequently, the development of high-activity non-noble metal catalysts has become a research hotspot. Zheng proved that heterogeneous Mo_3 single-cluster catalysts supported on nitrogen-doped graphene can use for robust electrochemical nitrogen reduction [15]. Ma compared a series of transition metals $TM_3@BN$ (TM = V, Fe, Mo, W) [14], and found that Mo_3 is an ideal NRR catalyst, which has the same catalytic ability as noble metal Au at the same time of low economic price.

The selection of catalyst carriers is equally important. From the perspective of different carriers' structural dimensions, common catalyst carriers include framework materials [28], two-dimensional lamellar materials (such as graphene, carbon nitrides, and transition metal carbides/nitrides) [25–27,29], *etc*. Hollow structural materials possess cavities in their structures, which

* Corresponding authors at: State Key Laboratory of Structural Chemistry, Fujian Institute of Research on the Structure of Matter, Chinese Academy of Sciences, Fuzhou 350002, China.
E-mail addresses: fwh@fjirsm.ac.cn (W. Fang), lqh2382@fjirsm.ac.cn (Q. Li).
[1] These authors contributed equally to this work.

https://doi.org/10.1016/j.cclet.2023.108604
1001-8417/

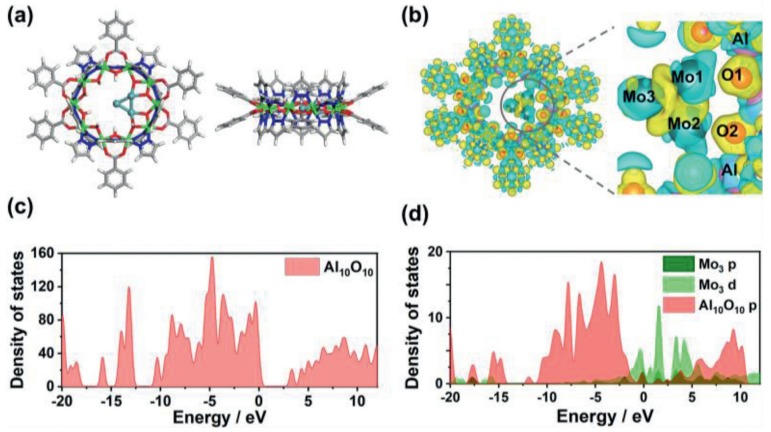

Fig. 1. (a) Structure diagram of $Mo_3@Al_{10}O_{10}$. (b) Charge density difference for $Mo_3@Al_{10}O_{10}$. (c, d) Density of states diagram of $Al_{10}O_{10}$ and $Mo_3@Al_{10}O_{10}$.

can prolong the residence time of N_2, enrich the reaction intermediates and shorten the electron transport path while stabilizing and exposing the active sites of the catalyst, thereby further enhancing its NRR activity [30]. Therefore, reasonable design of the pore size is very important. Pores with extremely small size are difficult for reactants to enter into the cavity [31], and are not conducive to anchoring catalytic active sites. Hollow structural materials with large specific area and high stability are suitable carriers. However, the hollow structure still has the problem of relying on the template method to synthesize, and it is difficult to obtain a precise and controllable structure. Crystalline aluminum-oxo clusters (AlOCs) possess precise molecular structure and excellent designability, which provide an ideal platform to study the catalytic effect. Zhang's group has reported a series of crystalline aluminum molecular rings with regular wheel-like structures [32], having the advantages of facile preparation [33], tunable sizes [34], and easy assembly [35]. Based on its size-adjustable cavities which can be used to nest metal clusters, aluminum molecular rings are an excellent catalyst carrier model.

Herein, we perform theoretical NRR calculations based on the largest aluminum-pyrazole ring $Al_{10}(OH)_{10}(BA)_6(PZ\text{-}CH_3)_{14}$ (AlOC-69; BA = benzoate; PZ-CH_3 = 4-methylpyrazole) to date. To simplify the calculation, the methyl groups on the pyrazoles are further replaced by H, constructing $Al_{10}O_{10}$. The d-orbitals of Mo and the p-orbitals of $Al_{10}O_{10}$ have formed stable Mo-O bonds, loading Mo_3 into the center of $Al_{10}O_{10}$. DFT calculations show that $Mo_3@Al_{10}O_{10}$ can activate N_2 with a more suitable activation energy of the electrochemical NRR and can suppress the generation of the hydrogen evolution side reaction. The results show that $Mo_3@Al_{10}O_{10}$ has catalytic performance comparable to that of noble metal catalysts and is a kind of good electrochemical NRR catalyst, providing a new approach for the design of efficient NRR catalysts with a novel structure.

To determine the stable structure of $Mo_3@Al_{10}O_{10}$, several initial configurations were considered and the most stable configuration obtained after optimization is shown in Fig. 1a. The optimized structure of Mo_3 is an approximately isosceles triangle, and two molybdenum atoms coordinate with two adjacent oxygen atoms in $Al_{10}O_{10}$ are approximately in parallel, forming two Mo-O bonds.

The bond lengths of Mo1-Mo2, Mo1-Mo3, and Mo2-Mo3 are 2.375 Å, 2.296 Å, and 2.314 Å, respectively, and the bond lengths of Mo1-O1 and Mo2-O2 are 2.117 Å and 2.110 Å, respectively. The overall structure of $Al_{10}O_{10}$ has not undergone significant deformation. Thermodynamic stability is an important indicator of catalytic activity, and the strong interaction between catalyst and carrier can avoid the migration of metal atoms. The calculated formation free energy of $Mo_3@Al_{10}O_{10}$ carrier is −0.76 eV. The result shows that there is a strong interaction between Mo_3 and $Al_{10}O_{10}$, which shows Mo_3 can be stabilized on the surface of the carriers.

To gain deeper insight into the stability of $Mo_3@Al_{10}O_{10}$, its electronic structures were further analyzed. The charge density difference of $Al_{10}O_{10}$ before and after adsorbed Mo_3 was calculated. As shown in Fig. 1b, the yellow and cyan lobes represent the accumulation and consumption of electrons in this area. It can be found that the Mo_3 surface is mainly characterized by the reduction of electron density and the presence of positive electron charge, while the adjacent two oxygen surfaces have electron accumulation, which can prove that there is an obvious interaction between Mo-O. It proves that the Mo_3 group can be stably adsorbed on $Al_{10}O_{10}$. Moreover, by observing the density of states (DOS) diagram before and after adsorption, as shown in Figs. 1c and d, both the d-orbitals of Mo_3 and the p-orbitals of $Al_{10}O_{10}$, whether above or below the Fermi level, have a strong hybridization effect. It proves that there is an interaction between the d-orbitals of Mo_3 and the p-orbitals of $Al_{10}O_{10}$. This electron transformation enables Mo_3 to firmly coordinate with $Al_{10}O_{10}$ and form a stable catalytic structure.

The adsorption and activation of N_2 on the catalyst is an important step in the whole NRR reaction process. The adsorption configuration and adsorption strength will directly affect the subsequent hydrogenation process. Through comparing the results of different structural optimization, the most stable configuration can be obtained (Fig. 2a). Through calculation, it is found that different from the end-on adsorption type of other metal catalysts, $Mo_3@Al_{10}O_{10}$ adopts the side-on adsorption type at the upper of two Mo atoms. Compared with end-on adsorption (−0.90 eV), side-on adsorption has higher adsorption energy (−1.08 eV) and higher stability. At the same time, side-on adsorption can better activate N_2 molecules. The bond lengths of Mo1-N1 and Mo3-N2 are 2.039 Å and 1.912 Å respectively. Nitrogen-nitrogen triple bond (N≡N) in N_2 is weakened and extends from the original 1.105 Å to 1.261 Å, achieving the effect of activation.

The charge transfer mode can be analyzed from the charge density difference after N_2 adsorption. As shown in Fig. 2b, N_2 is the electron acceptor in general, but a small decrease in charge density can also be seen between N≡N, which indicates that the electron transfer between N_2 and Mo_3 is not unidirectional, and it will also feed back to Mo_3 when N_2 gets electrons. There are simultaneous two transfers of electrons, from the occupied σ-orbital electrons of N_2 to the empty d-orbital of Mo, and from the occupied d-orbital of Mo to the π-antibonding-orbital of N_2. The analysis of DOS (Fig. 2c) and molecular orbital of N_2-Mo_3 (Fig. 2d) also further proves that there is a strong interaction between N-Mo, and the p-orbitals of N overlap with the d-orbitals of Mo to form bonds. On this basis,

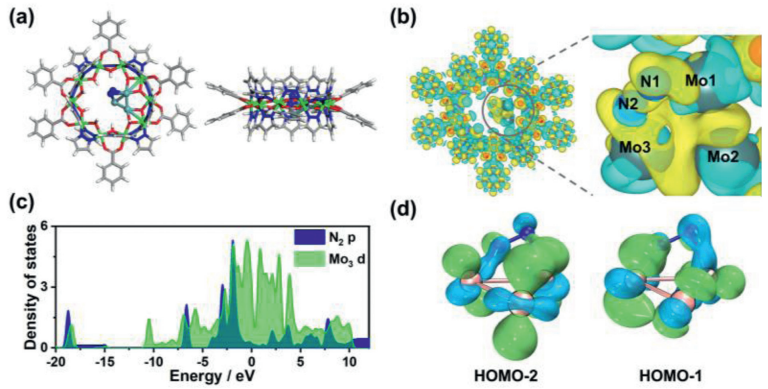

Fig. 2. (a) Structure diagram of adsorption of N_2 on $Mo_3@Al_{10}O_{10}$. (b) Charge density difference of the adsorption of N_2 on $Mo_3@Al_{10}O_{10}$. (c) Density of states diagram of Mo d-orbitals and N_2 p-orbitals of N_2 adsorbed $Mo_3@Al_{10}O_{10}$. (d) Molecular orbital of N_2-Mo_3.

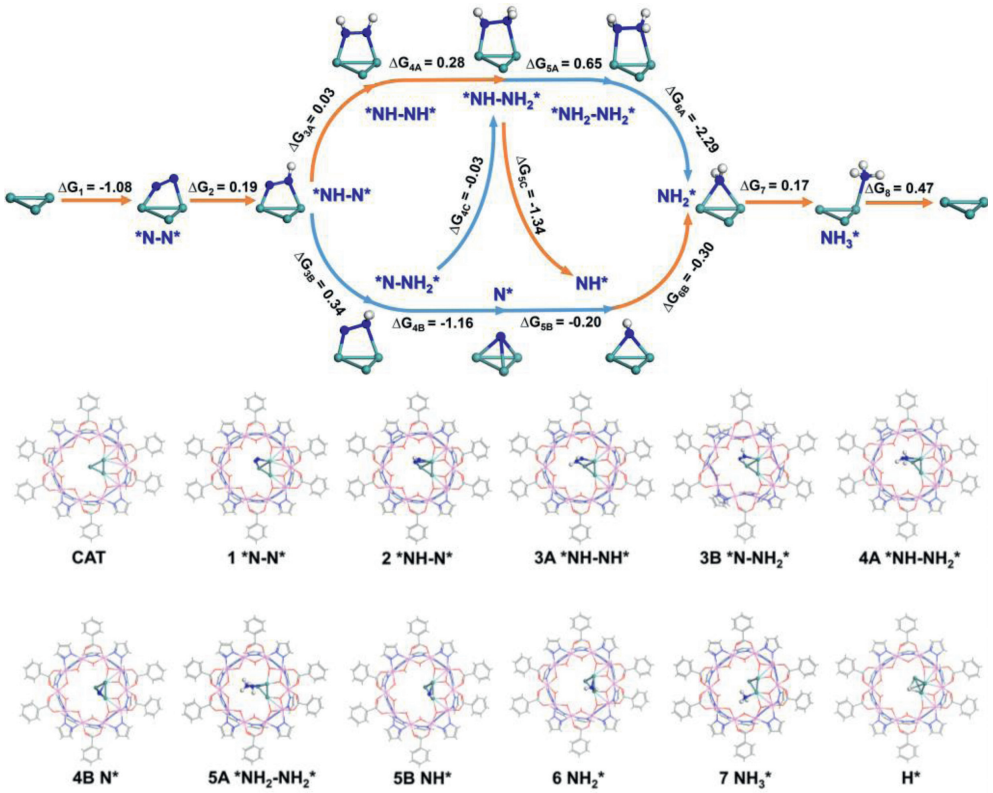

Fig. 3. Reaction intermediates in the electroreduction of N_2 to NH_3 on $Mo_3@Al_{10}O_{10}$ surface, with the corresponding ΔG (eV) in each step.

the adsorbed N_2 molecules are fully activated, and the first hydrogenation reaction is relatively easy to achieve.

By comparing different N_2 reduction reaction modes, it is difficult to directly break N≡N under mild conditions. Consequently, NRR in this system is carried out in association mode. N_2 is adsorbed on the surface of $Mo_3@Al_{10}O_{10}$ to carry out the hydrogenation reaction before breaking N≡N to generate NH_3. The Gibbs free energies of various paths without an applied electric field are calculated. As shown in Fig. 3, the free energy of adsorption of N_2 adsorbed at $Mo_3@Al_{10}O_{10}$ is −1.08 eV, indicating that this is a spontaneous thermodynamic process. The free energy of the process of forming *NH-N* intermediate is 0.19 eV, which is a non-spontaneous process. In the second hydrogenation process, 3A has lower free energy than 3B, which means process 3A is more energetically advantageous, and alternately H bonds on two N to generate *NH-NH* intermediate. *NH-NH* interacts with the third H to form *NH-NH_2*. This process requires the highest energy, 0.28 eV, which is the limiting step of the total reaction. Then *NH-NH_2* interacts with the fourth H and compared with process 5A adding on N2 to generate *NH_2-NH_2* (0.65 eV), the free energy of the process 5C adding on N1 to generate the first NH_3 is negative (−1.34 eV), which is thermodynamic spontaneous, leaving the NH* intermediate. NH* then interacts with the fifth and sixth H to form NH_2* intermediate and the second NH_3*.

The limiting potential (U_L) is given by $-\max(\Delta G)/e$, where ΔG is the free energy of each elemental protonation step in the NRR progress. As shown in Fig. 4a, only −0.28 V electric potentials are needed to make each step of the hydrogenation reaction become a thermodynamic spontaneous process, which is much lower than that of the most report (Fig. 4c and Table S6 in Supporting information) [7,14,18,29]. Since HER will consume H to generate H_2, which is the main competitive reaction of NRR, the presence of

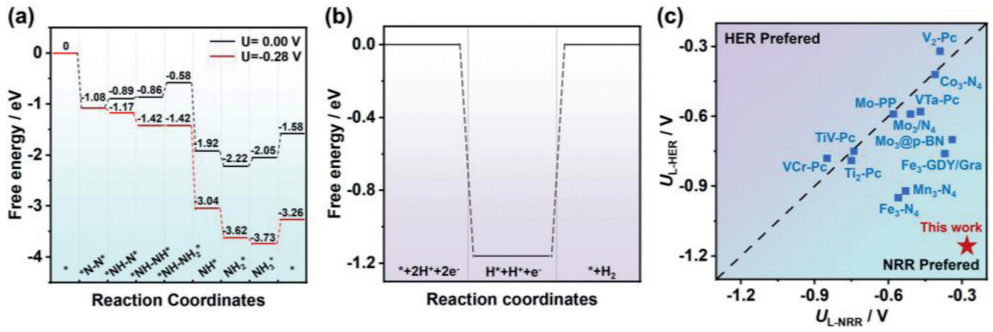

Fig. 4. (a) The calculated Gibbs free energy diagrams of the NRR on $Mo_3@Al_{10}O_{10}$ at different applied potentials. (b) Gibbs free energy diagrams of the HER on $Mo_3@Al_{10}O_{10}$. (c) Comparison of limiting potentials (U_L) in this work and those of previous reports.

HER will reduce the Faraday efficiency as well as the selectivity of NH_3. Therefore, the free energy of HER on $Mo_3@Al_{10}O_{10}$ was calculated as shown in Fig. 4b, it can be found that the energy barrier for the Heyrovsky step is 1.16 eV, which is far larger than the free energy of NRR (0.28 eV). Consequently, NH_3 is the main product on $Mo_3@Al_{10}O_{10}$, showing excellent selectivity.

In the present work, the largest aluminum-pyrazole ring (AlOC-69) to date was synthesized and combined with Mo_3 to produce a promising NRR catalyst. The calculated formation energy (−0.76 eV) and the electron transfer between Mo-O show the strong interaction between Mo_3 and $Al_{10}O_{10}$, demonstrating that Mo_3 can be stabilized at the carrier surface. Meanwhile, $Mo_3@Al_{10}O_{10}$ is an excellent NRR catalyst. The strong interaction between the p-orbital of N and the d-orbital of Mo makes the adsorbed N_2 molecule fully activated, and the first hydrogenation reaction occurs easily. During the whole process, the protonation of *NH-NH* to *NH-NH_2* is the limiting step with the maximum ΔG value of 0.28 eV, which is much smaller than competing HER (1.16 eV), showed promising catalytic selectivity. The precise molecular structure provides the basis for studying its structure-activity relationship and this novel structure breaks through the limitations of catalyst carriers, opening a new path to advance the sustainable production of NH_3.

Declaration of competing interest

The authors declare that they have no known competing financial interests or personal relationships that could have appeared to influence the work reported in this paper.

Acknowledgments

This work is supported by the National Natural Science Foundation of China (Nos. 92161105 and 92061104), Natural Science Foundation of Fujian Province (Nos. 2021J06035 and 2021J01525) and Youth Innovation Promotion Association CAS (No. Y2021081).

Supplementary materials

Supplementary material associated with this article can be found, in the online version, at doi:10.1016/j.cclet.2023.108604.

References

[1] T. Spatzal, K.A. Perez, O. Einsle, J.B. Howard, D.C. Rees, Science 345 (2014) 1620–1623.
[2] R.F. Service, Science 345 (2014) 610 -610.
[3] K.A. Brown, D.F. Harris, M.B. Wilker, et al., Science 352 (2016) 448–450.
[4] F. Bozso, G. Ertl, M. Weiss, J. Catal. 50 (1977) 519–529.
[5] M. Kitano, Y. Inoue, Y. Yamazaki, et al., Nat. Chem. 4 (2012) 934–940.
[6] C.J.M. van der Ham, M.T.M. Koper, D.G.H. Hetterscheid, Chem. Soc. Rev. 43 (2014) 5183–5191.
[7] L. Zhang, X. Ji, X. Ren, et al., Adv. Mater. 30 (2018) e1800191.
[8] C. Ling, Y. Zhang, Q. Li, et al., J. Am. Chem. Soc. 141 (2019) 18264–18270.
[9] Y. Wang, N. Yang, X. Xin, et al., Chin. Chem. Lett. 34 (2023) 107841.
[10] M.M. Shi, D. Bao, B.R. Wulan, et al., Adv. Mater. 29 (2017) 1606550.
[11] M. Nazemi, S.R. Panikkanvalappil, M.A. El-Sayed, Nano Energy 49 (2018) 316–323.
[12] V. Kordali, G. Kyriacou, C. Lambrou, Chem. Commun. (2000) 1673–1674.
[13] S. Licht, B. Cui, B. Wang, et al., Science 345 (2014) 637–640.
[14] S. Gao, Z. Ma, C. Xiao, et al., J. Mater. Sci. Technol. 108 (2022) 46–53.
[15] G. Zheng, L. Li, Z. Tian, X. Zhang, L. Chen, J. Energy Chem. 54 (2021) 612–619.
[16] C. Cui, H. Zhang, R. Cheng, B. Huang, Z. Luo, ACS Catal. 12 (2022) 14964–14975.
[17] X.L. Ma, M. Li, J.B. Lu, C.Q. Xu, J. Li, Chin. J. Struct. Chem. 41 (2022) 2212080–2212088.
[18] X. Liu, Y. Jiao, Y. Zheng, M. Jaroniec, S.Z. Qiao, J. Am. Chem. Soc. 141 (2019) 9664–9672.
[19] X. Yu, P. Han, Z. Wei, et al., Joule 2 (2018) 1610–1622.
[20] X. Yang, K. Li, D. Cheng, et al., J. Mater. Chem. A 6 (2018) 7762–7769.
[21] C. Zhao, S. Zhang, M. Han, et al., ACS Energy Lett. 4 (2019) 377–383.
[22] J. Yu, J. Li, X. Zhu, et al., ChemElectroChem 6 (2019) 2215–2218.
[23] T. Xu, J. Liang, Y. Wang, et al., Nano Res. 15 (2022) 1039–1046.
[24] Y.B. Li, Y.P. Liu, J. Wang, Y.L. Guo, K. Chu, Inorg. Chem. Front. 7 (2020) 455–463.
[25] J. Wang, M. Shi, G. Yi, et al., Chin. Chem. Lett. 33 (2022) 4623–4627.
[26] H.Q. Yin, L.L. Yang, H. Sun, et al., Chin. Chem. Lett. 34 (2023) 107337.
[27] S. Wu, M. Zhang, S. Huang, et al., Chin. Chem. Lett. 34 (2023) 107282.
[28] H.K. Lee, C.S.L. Koh, Y.H. Lee, et al., Sci. Adv. 4 (2018) eaar3208.
[29] X. Wang, Q. Zhang, W. Hao, et al., J. Mater. Chem. A 10 (2022) 15036–15050.
[30] C. Xue, X. Zhou, X. Li, et al., Adv. Sci. 9 (2022) 2104183.
[31] M. Nazemi, M.A. El-Sayed, J. Phys. Chem. Lett. 9 (2018) 5160–5166.
[32] Y. Li, C. Zheng, S.T. Wang, et al., Angew. Chem. Int. Ed. 61 (2022) e202116563.
[33] S.T. Wang, Y.J. Liu, C.C. Feng, W.H. Fang, J. Zhang, Aggregate 4 (2023) e264.
[34] L. Geng, C.H. Liu, S.T. Wang, W.H. Fang, J. Zhang, Angew. Chem. Int. Ed. 59 (2020) 16735–16740.
[35] S. Yao, W.H. Fang, Y. Sun, S.T. Wang, J. Zhang, J. Am. Chem. Soc. 143 (2021) 2325–2330.